Detailed chemical kinetic modeling of JP-10 (exo-tetrahydrodicyclopentadiene) high-temperature oxidation: Exploring the role of biradical species in initial decomposition steps

ARTICLE *in* INTERNATIONAL JOURNAL OF CHEMICAL KINETICS · MARCH 2012

Impact Factor: 1.52 · DOI: 10.1002/kin.20702

7 AUTHORS, INCLUDING:

Jorge Aguilera-Iparraguirre
Harvard University
17 PUBLICATIONS **176** CITATIONS
SEE PROFILE

Jesse Lutz
Durham University
12 PUBLICATIONS **163** CITATIONS
SEE PROFILE

Hsi-Wu Wong
University of Massachusetts Lowell
37 PUBLICATIONS **455** CITATIONS
SEE PROFILE

Oluwayemisi O. Oluwole
ANSYS
22 PUBLICATIONS **211** CITATIONS
SEE PROFILE

Detailed Chemical Kinetic Modeling of JP-10 (*exo*-Tetrahydrodicyclopentadiene) High-Temperature Oxidation: Exploring the Role of Biradical Species in Initial Decomposition Steps

GREGORY R. MAGOON,[1] JORGE AGUILERA-IPARRAGUIRRE,[1] WILLIAM H. GREEN,[1] JESSE J. LUTZ,[2] PIOTR PIECUCH,[2] HSI-WU WONG,[3] OLUWAYEMISI O. OLUWOLE[3]

[1]*Department of Chemical Engineering, Massachusetts Institute of Technology, Cambridge,* MA 02139
[2]*Department of Chemistry, Michigan State University, East Lansing,* MI 48824
[3]*Aerodyne Research, Inc., Billerica,* MA 01821-397

Received 6 June 2011; revised 30 September 2011, 23 October 2011; accepted 24 October 2011

DOI 10.1002/kin.20702
Published online 24 January 2012 in Wiley Online Library (wileyonlinelibrary.com).

ABSTRACT: The initial pathways of JP-10 (*exo*-tetrahydrodicyclopentadiene) decomposition are expected to have a significant effect on combustion and pyrolysis behavior of the fuel, affecting, for example, product distribution and ignition delay. Modeling of JP-10 decomposition should capture these initial decomposition processes as accurately as possible. Two classes of computational approaches have been applied to study intramolecular disproportionation—an important class of reactions in the initial stages of JP-10 decomposition: (1) the second-order,

Correspondence to: William H. Green; e-mail: whgreen@mit.edu.

Contract grant sponsor: Naval Air Warfare Center.
Contract grant number: N68335-10-C-0534.
Contract grant sponsor: Chemical Sciences, Geosciences and Biosciences Division, Office of Basic Energy Sciences, Office of Science, U.S. Department of Energy.
Contract grant number: DE-FG02-01ER15228.
Supporting Information is available in the online issue at wileyonlinelibrary.com.

multiconfigurational, quasidegenerate perturbation theory employing the complete active space self-consistent field (CASSCF) reference; and (2) the size-extensive, left-eigenstate, completely renormalized (CR) coupled-cluster (CC) method with singles, doubles, and noniterative triples, termed CR-CC(2,3), capable of describing reaction pathways involving biradicals. Applying higher levels of theory to points along the CASSCF reaction paths, the barriers to intramolecular disproportionation are much smaller and some barriers appear to vanish. The conventional ring-opening + disproportionation pathway is compared with an alternative concerted reaction pathway. Overall, this investigation has yielded insights into alkyl disproportionation and ring-opening reactions that may be of more general use in chemical kinetic modeling. © 2012 Wiley Periodicals, Inc. Int J Chem Kinet 44: 179–193, 2012

INTRODUCTION/MOTIVATION

JP-10 (*exo*-tetrahydrodicyclopentadiene) (see Fig. 1) is an important fuel in military applications, particularly in air-breathing propulsion. Its many desirable properties include high-energy density, high heat capacity, and low freezing point. Significant ongoing research is focused on the development of ramjet, scramjet, and pulse detonation engines that burn JP-10 fuel [1–11]. Although JP-10 is "simpler" than other jet propulsion fuels in that it is essentially a single-component fuel, its complex high-temperature decomposition chemistry is still not well understood. Many experimental and computational studies have been conducted by the research and development community in an effort to develop an improved understanding of JP-10 decomposition chemistry [5,8].

Herbinet et al. investigated the suspected important role of biradicals in the initial phases of JP-10 decomposition [8]. In particular, they looked at the behavior of biradicals formed by carbon–carbon bond homolysis in JP-10. They discussed how these biradicals can participate in intramolecular disproportionation reactions (in which one radical site in the molecule abstracts a hydrogen atom from the carbon adjacent to a second radical site to form a carbon–carbon double bond) and identified the important role of these intramolecular disproportionation reactions in pyrolytic decomposition of JP-10. Two of the reactions considered by Herbinet et al. are reaction (R1) and reaction (R2) shown below. (We follow the biradical reactant (BR)/MA notation of Herbinet et al.)

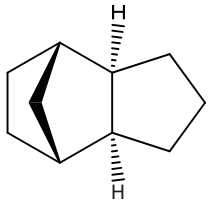

Figure 1 Molecular structure of JP-10.

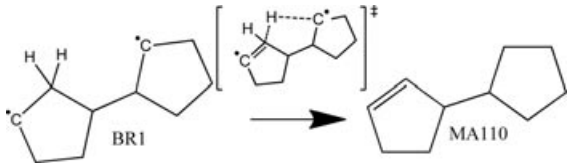

(R1)

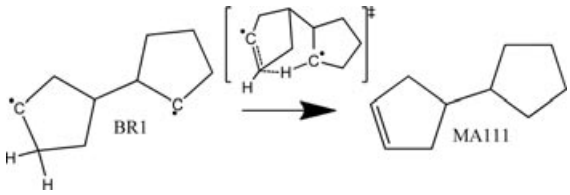

(R2)

Two pathways through reaction (R1) were identified by Herbinet et al., and the pathway shown, with a five-membered ring transition state, was proposed to have the lowest activation energy. Herbinet et al. proposed the scheme shown in Eq. (1) for estimating the activation energy for these intramolecular disproportionation reactions:

$$E_a = E_{a,ref} - SE_{ref\ cycle} + SE_{subpolycycle} \quad (1)$$

In Eq. (1), E_a is the activation energy and $E_{a,ref}$ is the activation energy for a reference *n*-alkdiyl intramolecular disproportionation with the transition state with the same ring size. The two SE terms refer to the ring strain energy for the reference cycle and the subpolycycle characteristics of the actual transition state. Using this approach to estimate the barriers, Herbinet et al. estimated rate constant expressions for reaction (R1) (with a five-membered ring transition state) and

reaction (R2) (with a [3.2.1] bicyclic ring transition state) as shown in Eqs. (2) and (3):

$$k_1(T) = 1.9 \times 10^{13}\mathrm{s}^{-1}\left(\frac{T}{1000\,\mathrm{K}}\right)^{1.0} \mathrm{e}^{\frac{-7.75\,\mathrm{kcal/mol}}{RT}} \quad (2)$$

$$k_2(T) = 1.9 \times 10^{13}\mathrm{s}^{-1}\left(\frac{T}{1000\,\mathrm{K}}\right)^{1.0} \mathrm{e}^{\frac{-19.85\,\mathrm{kcal/mol}}{RT}} \quad (3)$$

Previously, several of the authors of the present paper developed [10] a preliminary detailed JP-10 combustion mechanism using RMG, a software program for automated reaction mechanism generation [12]. The more recent refinements between the initial (v0.10) mechanism, published in [10], and the new (v0.19) mechanism, on which we rely in the present study, include the addition of important cyclic-C_5 chemistry as well as updates to thermodynamic and kinetic parameters based on ab initio calculations or the published literature; the refined (v0.19) mechanism includes 320 species reacting through 7740 elementary steps. The mechanism is included in the Supporting Information. With the exception of four BR1 pathways (where the estimates of Herbinet et al. were used), kinetic parameter estimates in the mechanism series from v0.10 [10] to v0.19 for this reaction class were estimated on-the-fly by RMG using a first-order approximation of the estimation scheme employed by Herbinet et al. where only the first term in their estimation procedure is retained, as shown in Eq. (4):

$$E_\mathrm{a} = E_{\mathrm{a,ref}} \quad (4)$$

Sensitivity analysis was performed with software based on SENKIN [13,14] for a constant-pressure adiabatic ignition simulation with a stoichiometric JP-10/air mixture starting at 1500 K and 1 atm, using the refined (v0.19) mechanism. Following the approach used by Davidson et al. in their experiments [5], ignition was modeled in our calculations as the time-to-peak CH composition. It was found that the ranked sensitivity coefficients, computed using

$$Z_i = \left|\frac{\partial y'_{\mathrm{CH}}(\tau_0)}{\partial \ln k_i}\right| \quad (5)$$

for kinetic parameters for multiple intramolecular disproportionation reactions (including reaction (R1)) appear among the top 2.5% (top 200) of all reactions in this large mechanism.[1]

This suggests that ignition delay can be sensitive to the kinetic parameter estimates for these intramolecular disproportionation reactions. Therefore, it will be important in future mechanism development to more accurately estimate activation energies for these reactions.

As the Herbinet et al. JP-10 intramolecular disproportionation estimates are not directly based on experiment or ab initio electronic structure calculations, independent estimates based directly on ab initio electronic structure calculations are desirable. The present paper represents an initial attempt in this direction.

METHODOLOGY

The investigation of the $C_{10}H_{16}$ system focused on reaction (R1) proceeding through a five-membered ring transition state, as considered by Herbinet et al. To validate the approach used for the $C_{10}H_{16}$ system and obtain additional insights, two smaller, simpler systems were studied as well, namely, a C_6H_{12} system, depicted in reaction (R3), and a C_3H_8 system, depicted in reaction (R4):

(R3)

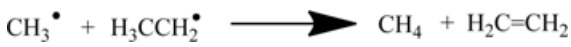

(R4)

It should be noted that the C_3H_8 system (reaction (R4)) is, unlike the others, a bimolecular reaction and is the smallest possible alkyl disproportionation reaction.

Each of the pathways characterizing reactions (R1), (R3), and (R4) was examined using the following three ab initio electronic structure methods: (i) the complete active space self-consistent field (CASSCF) approach [15–17], which is a multireference approach capable of describing nondynamical, many-electron correlation effects relevant to reaction mechanisms involving biradicals; (ii) the second-order multiconfigurational quasidegenerate perturbation theory (MCQDPT) employing the CASSCF reference [18,19], which is one of the commonly used multireference perturbation

[1]Note that y'_{CH} in this equation is the rate of change in the CH mass fraction and τ_0 refers to the ignition time for the unperturbed system. The partial derivative is evaluated holding the thermochemistry constant, i.e., both the forward and reverse rate coefficients of reaction i are adjusted by the same amount, so the equilibrium constant is not changed by the perturbation.

theory methods that corrects CASSCF results for the leading dynamical electron correlation effects; and (iii) the size-extensive, left-eigenstate, completely renormalized (CR) coupled-cluster (CC) method with singles, doubles, and noniterative triples, termed CR-CC(2,3) [20–23], exploiting the restricted Hartree–Fock reference, which is capable of providing an accurate and balanced description of nondynamical and dynamical correlation effects for chemical reaction pathways involving biradicals and single bond breaking with an ease of a black box, single-reference calculation through the use of suitably defined corrections to CCSD [24] energies [20–23,25–31]. The density functional theory (DFT) UB3LYP calculations [32,33] were also performed for comparison.

CASSCF, MCQDPT, and CR-CC(2,3) calculations used the 6-311G(d,p) basis set [34], whereas UB3LYP calculations used the CBSB7 basis set [35]. UB3LYP calculations were carried out using Gaussian09 [36], and CASSCF, MCQDPT, and CR-CC(2,3) calculations were performed using GAMESS [37,38]. In particular, the CR-CC(2,3) calculations used the routines developed at Michigan State University [20,39] that form a part of the GAMESS distribution. MacMolPlt [40] was used for visualization. All calculations were performed on the singlet potential energy surfaces. The core orbitals correlating with the 1s shells of the carbon atoms were frozen in post-SCF calculations.

As usual, each transition state was found as a saddle point (SP) on the potential energy surface of the indicated method, with one, and only one, imaginary frequency, and each minimum was identified as a stationary point with real frequencies only. Intrinsic reaction coordinate (IRC) calculations were performed with the same method as that used to determine transition states to confirm that each SP is connected to the appropriate minimum. The SPs, minima, and IRCs obtained in CASSCF optimizations were used in the subsequent single-point calculations at the higher MCQDPT and CR-CC(2,3) levels to examine the reliability of the CASSCF reaction profiles (this essentially constitutes a manual implementation of the established IRCMax method [41]). Generally, one expects the CASSCF calculations to provide a qualitatively correct information about reactive potential energy surfaces, particularly those involving biradical structures, but it often happens that barriers obtained with the CASSCF approach, which neglects dynamical correlation effects, disappear or are considerably reduced, when higher level ab initio methods that account for both the nondynamical and dynamical correlation effects, such as MCQDPT and CR-CC(2,3), are employed. This makes the MCQDPT and CR-CC(2,3) single-point calculations along the CASSCF IRCs and, whenever affordable, the MCQDPT and CR-CC(2,3) SP searches, to be of great significance in this study, because they can help us determine whether the barriers resulting from the CASSCF calculations are real. Based on earlier applications and benchmark studies, the MCQDPT and CR-CC(2,3) methods are capable of providing the results in the chemical (approximately 1 kcal/mol) accuracy range for the activation energies (see, e.g., [17, 29, 42]), but this would require using considerably larger basis sets than the 6-311G(d,p) basis set employed in this work, of at least triple zeta quality with multiple sets of d and f polarization functions and diffuse functions. Unfortunately, we could not afford using such basis sets in the MCQDPT and CR-CC(2,3) calculations performed in this study. The 6-311G(d,p) basis set used in the present work, which is of a triple zeta plus polarization quality, does not contain higher angular momentum (f and higher) and diffuse functions; so, based on the earlier studies, such as those presented in [29], we estimate that the errors resulting from our MCQDPT and CR-CC(2,3) calculations are on the order of about 2–3 kcal/mol, or so. Although this does not allow us to determine the relative energetics as precisely as for smaller molecules, for which MCQDPT and CR-CC(2,3) calculations using large basis sets are affordable, the main point of this study is an analysis of the significance of a balanced treatment of dynamical and nondynamical correlation effects, which the MCQDPT and CR-CC(2,3) approaches provide, on the key features of potential energy surfaces, such as activation barriers, which the lower order methods, such as CASSCF, which neglect dynamical correlation effects, may not properly describe. Such an analysis does not require using very large basis sets.

A four-electron, four-orbital active space (abbreviated "(4,4)") was used in CASSCF and MCQDPT calculations, and the active orbitals were chosen to be those of chemical significance for the intramolecular disproportionation process. The active orbitals for a representative example, corresponding to one of the transition states for reaction (R3) designated in the next section as TS3A, are plotted in Fig. 2. The figure shows that the molecular orbitals in the active space used in CASSCF(4,4) calculations correspond to the partially occupied molecular orbitals associated with breaking/forming bonds.

RESULTS AND DISCUSSION

Intramolecular Disproportionation

C_3H_8 System. The first system considered, C_3H_8, corresponding to reaction (R4), involves methyl + ethyl

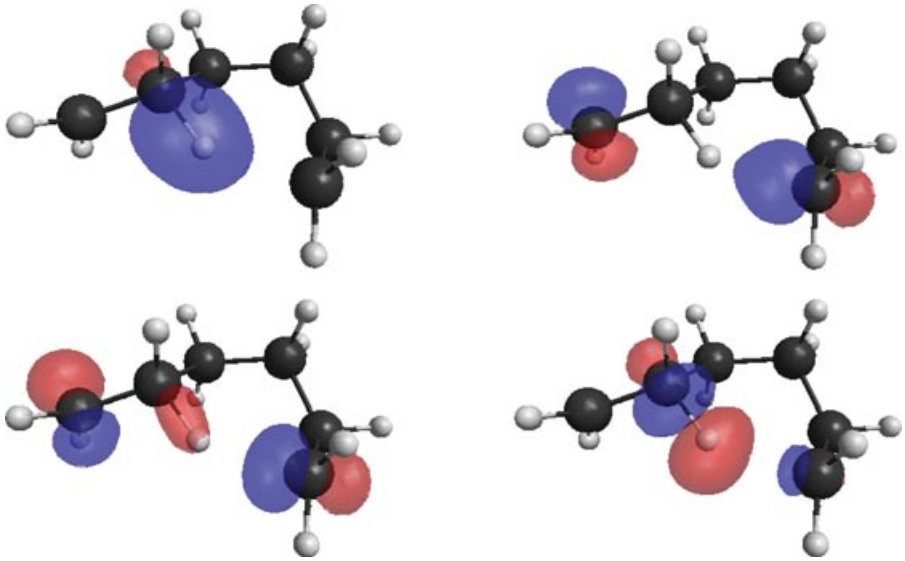

Figure 2 CASSCF(4,4) active orbitals for transition state TS3A of reaction (R3). [Color figure can be viewed in the online issue, which is available at wileyonlinelibrary.com.]

disproportionation and is the smallest possible alkyl disproportionation reaction, so we use it as an initial step in our way toward the full JP-10 study. The C_3H_8 system is small enough to enable us to explore the CR-CC(2,3) and MCQDPT potential energy surfaces with numerical energy gradients, in addition to calculating single-point CR-CC(2,3) and MCQDPT energies along the CASSCF(4,4) IRC pathways. This system has recently been studied by Mousavipour and Homayoon [43] and by Zhu et al. [44] The results of the CASSCF(4,4) calculations and the potential energy surface scans along the CASSCF(4,4)-optimized IRC leading to the methyl + ethyl reactants obtained with the higher level MCQDPT(4,4) and CR-CC(2,3) approaches are shown in Fig. 3. The various single-point energies calculated at the SP and reactant geometries obtained with CASSCF(4,4) are presented in Table I.

As shown in Fig. 3, the CASSCF(4,4) calculations show a well-pronounced barrier (of about 5 kcal/mol), whereas the CR-CC(2,3) single-point energy calculations along the CASSCF(4,4) IRC show only a tiny barrier (under 1 kcal/mol), well within the intrinsic error of the method, shifted toward the reactant side. The analogous single-point MCQDPT calculations do not show any barrier along the CASSCF(4,4) path. Also, our own calculations with UB3LYP confirmed the findings of Zhu et al., who observed the existence of a stable complex and an SP using that method [44]. Thus, this system shows four qualitatively different potential energy surfaces as the method is varied between CASSCF(4,4), CR-CC(2,3), MCQDPT(4,4), and UB3LYP. Owing to the small size of the system,

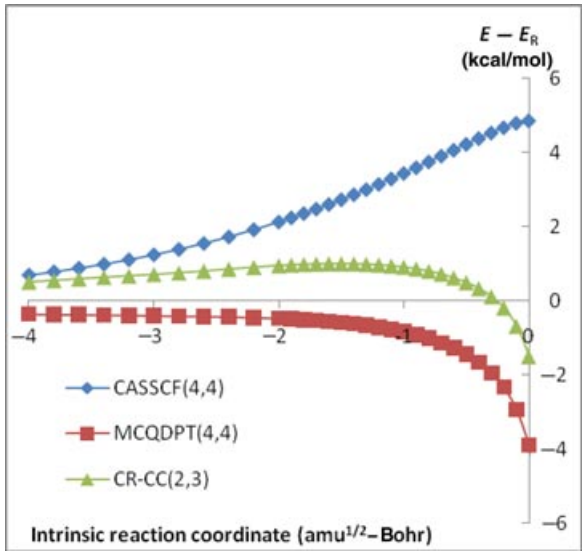

Figure 3 Energy profiles for reaction (R4) along the CASSCF(4,4) IRC, calculated at different levels of theory. In each case, the points correspond to selected structures on the relevant CASSCF(4,4)-optimized IRC, with the abscissa indicating the approximate IRC relative to the SP. The energies E characterizing the profile are reported relative to the energy of a noninteracting complex representing radical reactants identified by following the CASSCF(4,4) IRC (E_R). Note that although there is a CR-CC(2,3) barrier along this CASSCF(4,4) IRC path, further study suggested that there is a barrierless path for this reaction on the CR-CC(2,3) potential energy surface (see the text for details).

we could afford to search for an SP using numerical gradients of CR-CC(2,3) and MCQDPT(4,4); our efforts to find an SP using these two approaches were

Table I Total Electronic Energies at the Saddle Point (SP) and Reactant (R) Geometries Obtained in the CASSCF(4,4)/6-311G(d,p) Geometry Optimizations[a]

CASSCF(4,4)			MCQDPT(4,4)//CASSCF(4,4)				CR-CC(2,3)//CASSCF(4,4)			
SP	R	ABH = IBH	SP	R	ABH	IBH	SP	R	ABH	IBH
−0.192740	−0.200490	4.9	−0.630532	−0.624321	−3.9	0	−0.682549	−0.680137	−1.5	1.0

The table also reports the corresponding apparent barrier heights (ABH, in kcal/mol; calculated in each case as the difference between the appropriate energies at the SP and R geometries found with CASSCF(4,4)), and the IRC barrier heights (IBH, in kcal/mol; calculated in each case as the energy difference between the highest energy point along the CASSCF(4,4) IRC available, different for each method, and the corresponding energy at the CASSCF(4,4)-optimized R geometry), characterizing the CASSCF(4,4)/6-311G(d,p)-optimized reaction pathway representing reaction (R4).

[a]Total electronic energies are reported in Hartree. Each electronic energy E is reported as $(E + 118)$ Hartree.

unsuccessful, suggesting that this reaction is barrierless at higher levels of theory. This indicates a need to include the dynamical and nondynamical many-electron correlation effects in a balanced manner to obtain reliable reaction path energetics. The CR-CC(2,3) and MCQDPT methods describe both types of electron correlation effects in an accurate manner, eliminating the well-pronounced barrier resulting from the CASSCF(4,4) calculations, which include the relevant nondynamical correlations, but neglect dynamical correlation effects.

C_6H_{12} System. The second system, which is associated with the cyclohexane ring opening and which can be regarded as an intermediate between the previously discussed C_3H_8 case and JP-10, is the C_6H_{12} system, corresponding to reaction (R3). The C_6H_{12} system gives us an opportunity to relatively rapidly explore the MCQDPT(4,4) potential energy surface with numerical energy gradients. Three SPs were found for reaction (R3) (hexamethylene ↔ 1-hexene) using CASSCF(4,4). These SPs, labeled as TS3A, TS3B, and TS3C, are shown in Fig. 4.

Similar SPs were found with UB3LYP; two of these SPs (associated with SPs TS3A and TS3B) were considered by Sirjean et al. [45]. The results of the CASSCF(4,4) calculations and the potential energy surface scans along the CASSCF(4,4)-optimized IRCs leading from the SPs to the BRs obtained with the higher level MCQDPT(4,4) and CR-CC(2,3) approaches are shown in Fig. 5. The various single-point energies calculated at the SP and reactant geometries obtained with CASSCF(4,4) are presented in Table II.

The single-point energy calculations at the selected structures along the CASSCF(4,4) IRCs corresponding to the transition states TS3A, TS3B, and TS3C, found with CASSCF(4,4) and UB3LYP suggest no barriers or negligible barriers at the MCQDPT(4,4) and CR-CC(2,3) theory levels. In fact, all of our efforts to refine the CASSCF(4,4) SP geometries with numerical gradients of MCQDPT were unsuccessful, suggesting that these are not valid SPs at the MCQDPT level of theory. Although we were unable to perform similar SP searches with the CR-CC(2,3) method, the similarity of the MCQDPT and CR-CC(2,3) results shown in Fig. 5 and Table II strongly suggests that none of the transition states found with CASSCF(4,4) are valid SPs at the CR-CC(2,3) level either. This shows once again that lower order methods, such as CASSCF, which neglects dynamical correlations, and UB3LYP, which has well-known difficulties with an adequate description of nondynamical correlation effects and potential energy surfaces involving biradicals, cannot be used to obtain reliable reaction path energetics. One has to

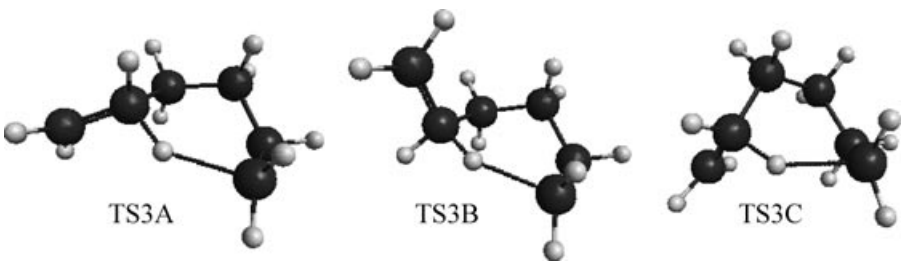

Figure 4 CASSCF(4,4) SPs for reaction (R3).

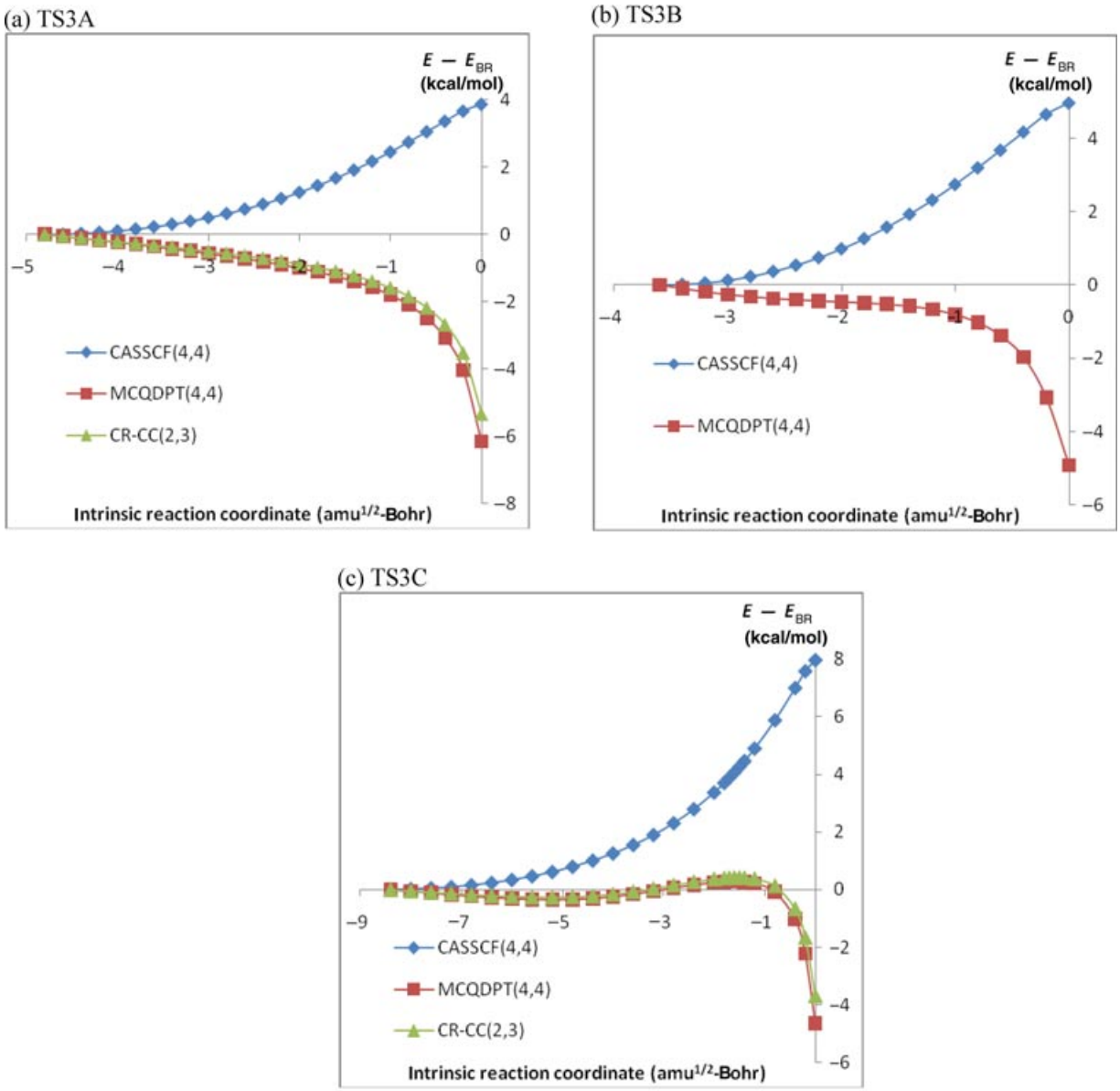

Figure 5 Energy profiles for reaction (R3) along the CASSCF(4,4) IRCs passing through the (a) TS3A, (b) TS3B, and (c) TS3C SPs, calculated at different levels of theory. In each case, the points correspond to selected structures on the relevant CASSCF(4,4)-optimized IRC, with the abscissa indicating the approximate IRC relative to the SP. The energies E characterizing each profile are reported relative to the corresponding IRC-connected biradical minimum (E_{BR}), which corresponds to the terminal point at the left.

include the relevant dynamical and nondynamical correlation effects in an accurate and balanced manner in the calculations, as is the case when the MCQDPT and CR-CC(2,3) approaches are employed, to obtain reasonable results. The absence of the well-pronounced barriers in the reaction profiles obtained by performing the single-point MCQDPT(4,4) and CR-CC(2,3) calculations along the CASSCF(4,4) IRC pathways suggests that the CBS-QB3 barrier (based on B3LYP geometries) of 3.85 kcal/mol used by Herbinet et al. (apparently based on the aforementioned study from Sirjean et al.) may be too high. Our efforts to optimize the corresponding BR minima (found at either CASSCF(4,4) or UB3LYP levels) to a stable MCQDPT(4,4) minimum energy configuration were unsuccessful as well. However, explorations of the C_6H_{12} system by Kiefer et al. [46] with CASPT2(2,2) produced a viable SP (more akin to the BRs than the

Table II Total Electronic Energies at the CASSCF(4,4)/6-311G(d,p)-Optimized Saddle Points (SP) and Biradical Reactant (BR) Minima[a]

	CASSCF(4,4)			MCQDPT(4,4)//CASSCF(4,4)				CR-CC(2,3)//CASSCF(4,4)			
IRC	SP	BR	ABH = IBH	SP	BR	ABH	IBH	SP	BR	ABH	IBH
TS3A	−0.161615	−0.167792	3.9	−1.042388	−1.032588	−6.1	0	−1.133733	−1.125251	−5.3	0
TS3B	−0.158028	−0.165924	5.0	−1.038881	−1.031050	−4.9	0	−1.131023	−1.123573	−4.7	N/C
TS3C	−0.155247	−0.167922	8.0	−1.040458	−1.033069	−4.6	0.3	−1.131659	−1.125778	−3.7	0.4

The table also reports the corresponding apparent barrier heights (ABH, in kcal/mol; calculated in each case as the difference between the appropriate energies at the SP and BR geometries found with CASSCF(4,4)), and the IRC barrier heights (IBH, in kcal/mol; calculated in each case as the energy difference between the highest energy point along the CASSCF(4,4) IRC available, different for each method, and the corresponding energy at the CASSCF(4,4)-optimized BR geometry), characterizing the three CASSCF(4,4)/6-311G(d,p) optimized reaction pathways representing reaction (R3).

N/C, not calculated in this work.

[a]Total electronic energies are reported in Hartree. Each electronic energy E is reported as $(E+234)$ Hartree.

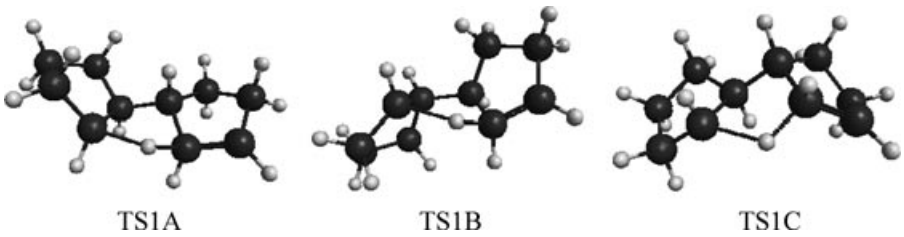

Figure 6 CASSCF(4,4) SPs for reaction (R1).

previously discussed CASSCF(4,4) and UB3LYP TS3 geometries) that was readily reoptimized to an SP at the MCQDPT(4,4) level of theory in this study. (The zero-point energy (ZPE)-uncorrected barrier was found to be 2.6 kcal/mol at the MCQDPT(4,4) level.) These results underscore the lack of reliability of CASSCF(4,4) and UB3LYP geometries for this type of reaction system.

$C_{10}H_{16}$ System. As in the case of the C_6H_{12} system discussed in the preceding subsection, three SPs, labeled TS1A, TS1B, and TS1C, were found for reaction (R1) using CASSCF(4,4), as shown in Fig. 6.

IRC calculations were performed to confirm that each SP connects the minima that correspond to the desired reactant and product species. Similar SP geometries, with similar IRCs, were found using UB3LYP. Higher level MCQDPT and CR-CC(2,3) single-point calculations that describe the dynamical as well as nondynamical correlation effects were performed at selected points along the CASSCF(4,4) IRC, and results are shown in Fig. 7 and Table III.

In analogy to the previously discussed C_3H_8 and C_6H_{12} systems, the potential energy surface scans along the CASSCF(4,4)-optimized IRCs obtained with the higher level MCQDPT(4,4) and CR-CC(2,3) approaches, shown in Fig. 7, suggest that the CASSCF calculations do not provide a reliable description of pathway energetics characterizing reaction (R1). This is particularly true in the case of the reaction pathway corresponding to the transition state TS1B, where CASSCF(4,4) predicts the existence of the well-pronounced activation barrier on the order of 8 kcal/mol, which nearly disappears in the MCQDPT(4,4) and CR-CC(2,3) calculations, mimicking the behavior we have seen with all three transition states for the C_6H_{12} case. The CASSCF(4,4) calculations include all of the relevant nondynamical correlation effects, but they neglect dynamical correlations and, as a result, produce the unphysical barrier in this case, which the MCQDPT(4,4) and CR-CC(2,3) approaches that describe the nondynamical as well as dynamical correlation effects eliminate. The inclusion of more active orbitals and more active electrons in the CASSCF calculations lowers the apparent TS1B barrier, which only reinforces the above observations. For example, the apparent TS1B barriers resulting from the CASSCF(6,6) and CASSCF(8,8) calculations are 6.6 and 5.3 kcal/mol, as opposed to about 8 kcal/mol obtained in the CASSCF(4,4) calculations. For the remaining two pathways, which correspond to transition states TS1A and TS1C, the barriers obtained in the CASSCF(4,4) calculations survive when the MCQDPT(4,4) and CR-CC(2,3) methods are employed, but we observe a significant barrier lowering when the dynamical correlation effects are taken into account

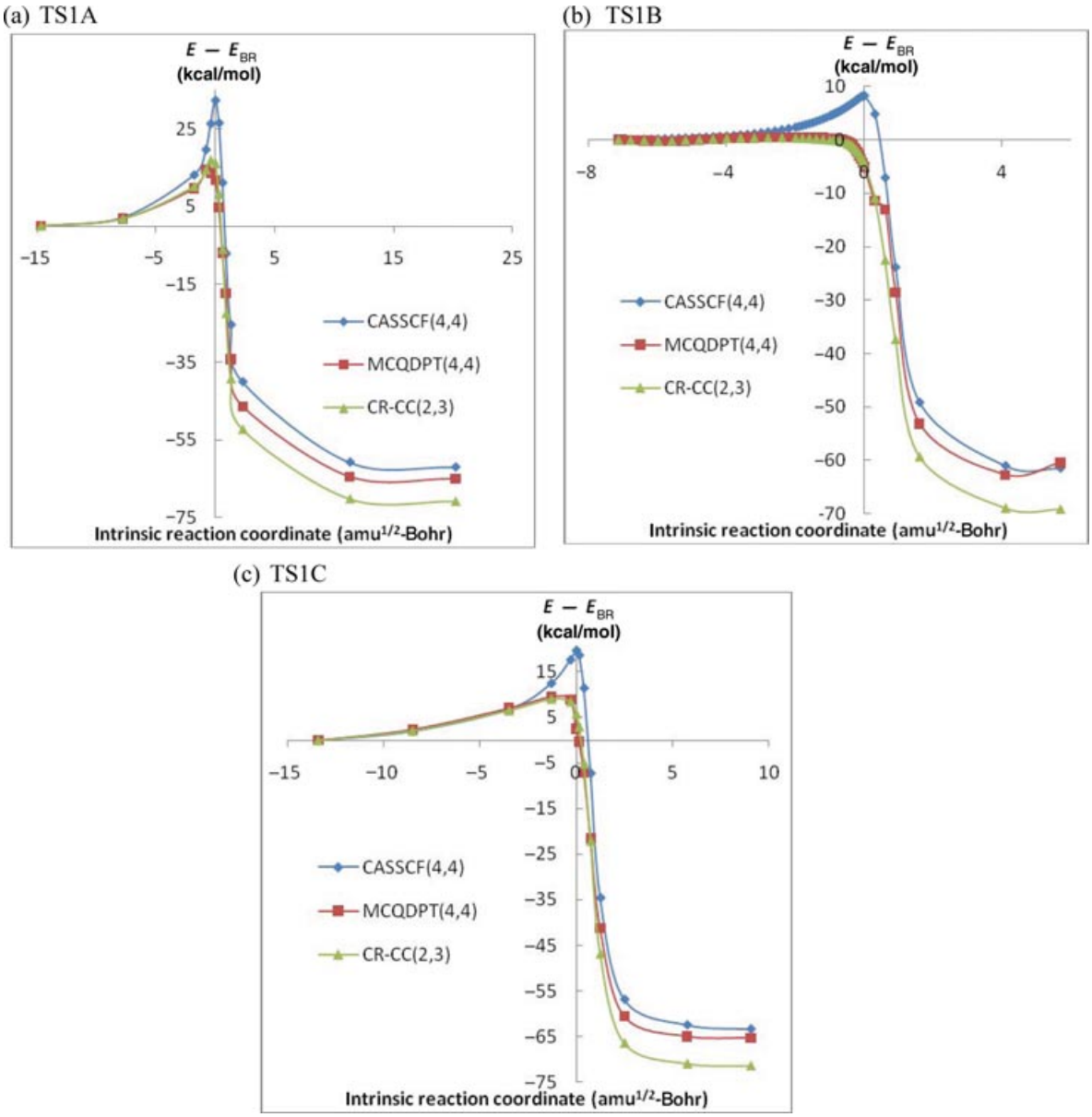

Figure 7 Energy profiles for reaction (1) along the CASSCF(4,4) IRCs passing through the (a) TS1A, (b) TS1B, and (c) TS1C SPs, calculated at different levels of theory. In each case, the points correspond to selected structures on the relevant CASSCF(4,4)-optimized IRC, with the abscissa indicating the approximate IRC relative to the SP. The energies E characterizing each profile are reported relative to the corresponding IRC-connected biradical minimum (E_{BR}), which corresponds to the terminal point at the left.

via MCQDPT(4,4) and CR-CC(2,3) (by a factor of about 2–3). Moreover, although we were unable to perform the SP optimizations using the MCQDPT and CR-CC(2,3) levels due to prohibitive costs of such calculations, a closer inspection of the energy profiles shown in Figs. 7a and 7c indicates that the transition states TS1A and TS1C shift toward the corresponding BR minima when the dynamical correlation effects are included via the MCQDPT and CR-CC(2,3) approaches. Last, but not least, although there are some differences between barrier heights resulting from the MCQDPT and CR-CC(2,3) calculations for the pathways involving the TS1A and TS1C transition states, these differences become smaller as the active space employed in the MCQDPT calculations becomes larger. For example, the apparent barrier height

Table III Total Electronic Energies at the CASSCF(4,4)/6-311G(d,p)-Optimized Saddle Points (SP) and Biradical Reactant Minima (BR)[a]

	CASSCF(4,4)			MCQDPT(4,4)//CASSCF(4,4)				CR-CC(2,3)//CASSCF(4,4)			
IRC	SP	BR	ABH = IBH	SP	BR	ABH	IBH	SP	BR	ABH	IBH
TS1A	−0.963522	−1.015185	32.4	−2.434862	−2.453652	11.8	14.6	−2.566955	−2.592631	16.1	17.0
TS1B	−1.000906	−1.014091	8.3	−2.468157	−2.459969	−5.1	0.5	−2.601343	−2.594176	−4.5	0.4
TS1C	−0.980512	−1.012022	19.8	−2.448613	−2.452571	2.5	9.6	−2.581793	−2.591074	5.8	9.1

The table also reports the corresponding apparent barrier heights (ABH, in kcal/mol; calculated in each case as the difference between the appropriate energies at the SP and R geometries found with CASSCF(4,4)), and the IRC barrier heights (IBH, in kcal/mol; calculated in each case as the energy difference between the highest energy point along the CASSCF(4,4) IRC available, different for each method, and the corresponding energy at the CASSCF(4,4)-optimized BR geometry), characterizing the three CASSCF(4,4)/6-311G(d,p) optimized reaction pathways representing reaction (R1).

[a]Total electronic energies are reported in Hartree. Each electronic energy E is reported as $(E + 387)$ Hartree.

corresponding to the transition state TS1A obtained in the MCQDPT(8,8) calculations is 13.1 kcal/mol. This is closer to 16.1 kcal/mol resulting from the CR-CC(2,3) calculations than the value of 11.8 kcal/mol obtained with MCQDPT(4,4). Similarly, the apparent barrier height corresponding to the transition state TS1C obtained in the MCQDPT(8,8) calculations, of 6.1 kcal/mol, is much closer to 5.8 kcal/mol resulting from the CR-CC(2,3) calculations than 2.5 kcal/mol obtained with MCQDPT(4,4). These similarities of the results for reaction (R1) obtained with the MCQDPT and CR-CC(2,3) approaches, which represent two independent quantum chemical methodologies, confirm once again that we cannot rely on the CASSCF approach alone in producing a reliable description of the reaction (R1) energetics.

It should be noted that the above results do not consider ZPE effects, but our conclusions would not change if these effects were included. Indeed, our CASSCF(4,4) calculations suggest that ZPE effects should uniformly lower the barriers by approximately 1.0 kcal/mol. Also, it is noted that the biradical that each of the three SPs connects to is a different CASSCF(4,4) minimum; the biradical minimum associated with TS1A has the lowest energy at the CASSCF(4,4) level, whereas the biradical minimum associated with TS1B has the lowest energy at MCQDPT(4,4) and CR-CC(2,3) levels. Calculations using a CASSCF(4,4) geometry for JP-10 also enabled an estimation of 0 K bond energy associated with carbon–carbon bond breaking to form the BR1 biradical associated with TS1A, producing values of 59, 75, and 81 kcal/mol for CASSCF(4,4), MCQDPT(4,4)//CASSCF(4,4), and CR-CC(2,3)//CASSCF(4,4), respectively (all with CASSCF(4,4) ZPE); these values are lower than the 0 K bond dissociation energy in ethane of about 88 kcal/mol [47].

Discussion/Kinetic Modeling of the $C_{10}H_{16}$ System. Overall, the above three systems illustrate method-dependent phenomenon in the potential energy surfaces of disproportionation reactions, with a strong indication toward the need to use higher level quantum chemistry approaches, such as MCQDPT or CR-CC(2,3), which are capable of describing dynamical as well as nondynamical electron correlation effects in an accurate and balanced manner, resulting in improved reaction energetics. In the context of the disproportionation reactions examined in this work, it is quite clear that the inclusion of dynamical many-electron correlation effects, in addition to nondynamical correlations, lowers or, in some cases, even eliminates the reaction barriers along paths determined using lower order (CASSCF) calculations.

To ascertain the influence of lower intramolecular disproportionation barriers on combustion behavior of JP-10, the activation energies of all intramolecular disproportionation reactions in the mechanism were dropped by 7.75 kcal/mol (the activation energy for reaction (R1) from the Herbinet approach) to a minimum of 0.0 kcal/mol. The resulting mechanism was labeled v0.19b, and ignition simulations were performed using the isobaric simulation feature in SENKIN, with ignition determined by the point with the highest CH mole fraction [13]. Ignition delay results for the unperturbed v0.19 and the perturbed v0.19b mechanisms were compared with experimental values of Davidson et al. [5], as shown in Fig. 8.

The results suggest that the activation energy perturbation has its biggest effect on the conditions with the longest ignition delay. In particular, for such conditions, the activation energy reduction appears to further delay ignition. One possible explanation for this is that the faster termination reaction of the biradical is depleting the (bi)radical pool, hence delaying the onset of ignition. The importance of these reactions at

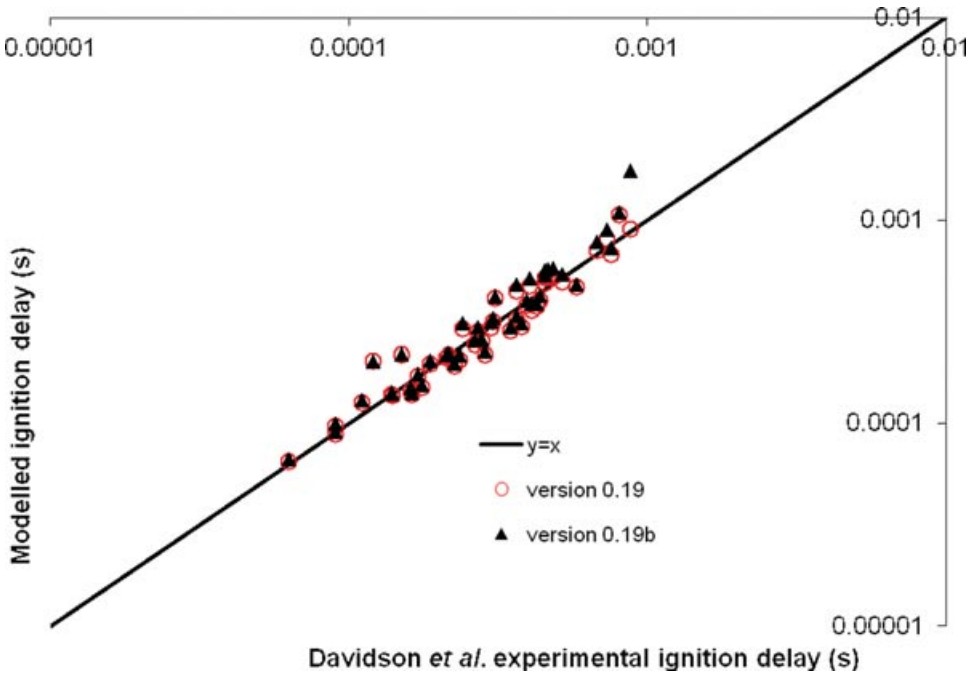

Figure 8 Parity plot comparing ignition delay from unperturbed and perturbed mechanisms (v0.19 and v0.19b, respectively) to experimental results of Davidson et al. [5]

conditions with longer ignition delay is supported by sensitivity analysis, which shows, for example, that reaction (R1) increases from an importance rank of 171 of 7740 reactions (again, computed based on the sensitivity metric defined by Eq. (5), discussed previously) at conditions corresponding to the point at the far left (1671 K, 1.05 atm, 0.20 mol% JP-10, 2.99 mol% O_2; remainder Ar) to a rank of 130 at the conditions corresponding to the point at the far right (1352 K, 8.69 atm, 0.20 mol% JP-10, 2.78 mole% O_2; remainder Ar).

Ring-Opening Pathways with Concerted Hydrogen Transfer

Background. The possibility of concerted reactions leading directly from ring to alkene, bypassing biradical intermediate, was also considered. There appears to be limited discussion of these pathways in the literature. An investigation of C_4H_8 by Ventura et al. [48] found that tetramethylene was not a stable structure when using the MR-AQCC approach [49], which is a size-extensive modification of the multireference configuration interaction (MRCI) method that takes both dynamical and nondynamical correlation effects into account. This would suggest that ring opening of cyclobutane leads directly to 1-butene without a biradical intermediate. Later, Kiefer et al. found a concerted pathway from cyclohexane to 1-hexene using CASPT2(2,2) with relatively low barrier, but concluded that the kinetics were not competitive with the biradical pathway due to a low Arrhenius prefactor [46].

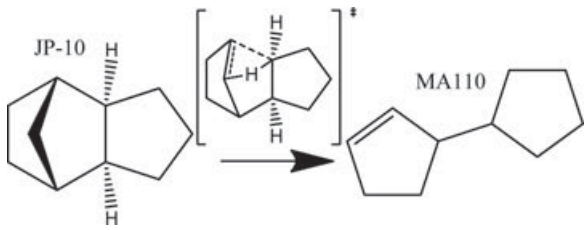

(R5)

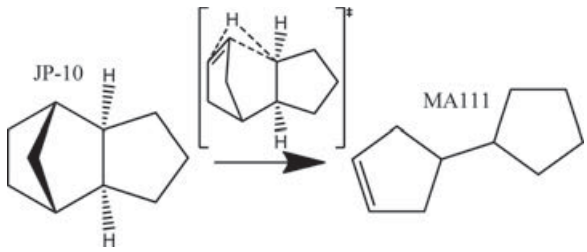

(R6)

DFT Calculations. Two SPs, labeled as TS5 and TS6, corresponding to a concerted JP-10↔MA110 reaction, have been found at the UB3LYP level. Our CBS-QB3 calculations, performed with Gaussian09,

Table IV CBS-QB3 Absolute and Relative Energetics for Reactions (R5) and (R6)

Species	CBS-QB3 (0 K) Energy (Hartree)	Barrier Height (kcal/mol)
JP-10	−389.881322	–
TS5	−389.702457	112.2
TS6	−389.754219	79.8

suggest a high barrier of more than 110 kcal/mol for TS5 and a lower barrier of about 80 kcal/mol for TS6 (see Table IV). The latter is comparable to the barrier of 77 kcal/mol estimated by Herbinet et al. for the ring opening of JP-10 to form BR1, which provides a rough indication that the concerted pathway could be competitive with the biradical pathway for JP-10 decomposition. Let us recall that CBS-QB3 is a composite approach for estimating complete basis set limit QCISD(T) results [35]. The existence of the TS5 and TS6 transition states has been reexamined using the CASSCF(4,4) approach. We could not find an SP similar to TS5 on the CASSCF(4,4) potential energy surface, which indicates the need for further examination if the TS5 structure is a real transition state, but the CASSCF(4,4) calculations confirmed the existence of the TS6 SP structure. Although higher level MCQDPT, CR-CC, or MRCI calculations could change these findings, the rather high barrier height corresponding to the TS6 structure indicates that this is, most likely, a real SP.

Table IV reports the CBS-QB3 results (electronic energy + ZPE) for the JP-10 reactant and TS5 and TS6 SPs on the UB3LYP surface. The UB3LYP geometries of TS5 and TS6 are shown in Fig. 9.

Using CANTHERM [50], a modified Arrhenius fit was obtained for each of these reactions based on CBS-QB3 results and transition state theory. This led to the rate parameter estimates for reactions (R5) and (R6) shown in Eqs. (6) and (7), respectively:

$$k_5(T) = 2.54 \times 10^{11}\mathrm{s}^{-1}\left(\frac{T}{1000\,\mathrm{K}}\right)^{6.88} \mathrm{e}^{\frac{-99.31\,\mathrm{kcal/mol}}{RT}} \tag{6}$$

$$k_6(T) = 9.1 \times 10^{14}\mathrm{s}^{-1}\left(\frac{T}{1000\,\mathrm{K}}\right)^{1.23} \mathrm{e}^{\frac{-80.34\,\mathrm{kcal/mol}}{RT}} \tag{7}$$

It is possible that additional concerted JP-10 decomposition pathways exist that were not identified in this study.

Kinetics Implications. An attempt was made to assess the importance of the reaction (R6) concerted pathway relative to the biradical pathways considered by Herbinet et al. For the biradical pathways, kinetic parameters for the JP-10 ↔ BR1 reaction, reaction (R1) (both pathways), and reaction (R2) were taken from Herbinet et al. Thermochemistry for JP-10 is based on the Herbinet et al. values, and thermochemistry for BR1 is based on the values from Herbinet et al. estimated using quantum methods. Two approaches were used to calculate an effective rate constant for the two-step biradical pathway. One approach was to assume rapid equilibrium between BR1 and JP-10. The second approach was to apply the pseudo–steady-state approximation to BR1. A comparison of these effective rates with the reaction (R6) concerted pathway rate (computed as described previously) is shown in Fig. 10.

The comparison suggests that the concerted pathway is competitive at very low temperatures, but the biradical pathway to MA110 dominates at higher temperatures of interest to combustion. Even so, the concerted pathway to MA111 appears to be faster than the corresponding biradical pathway for temperatures less than 2000 K. The lower magnitude slope for the

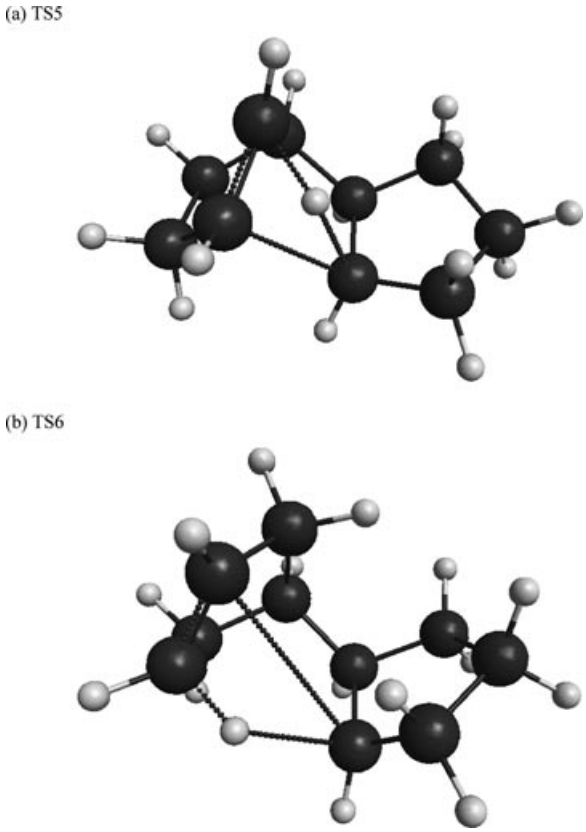

Figure 9 UB3LYP SP geometries for reactions (R5) and (R6): (a) TS5 and (b) TS6.

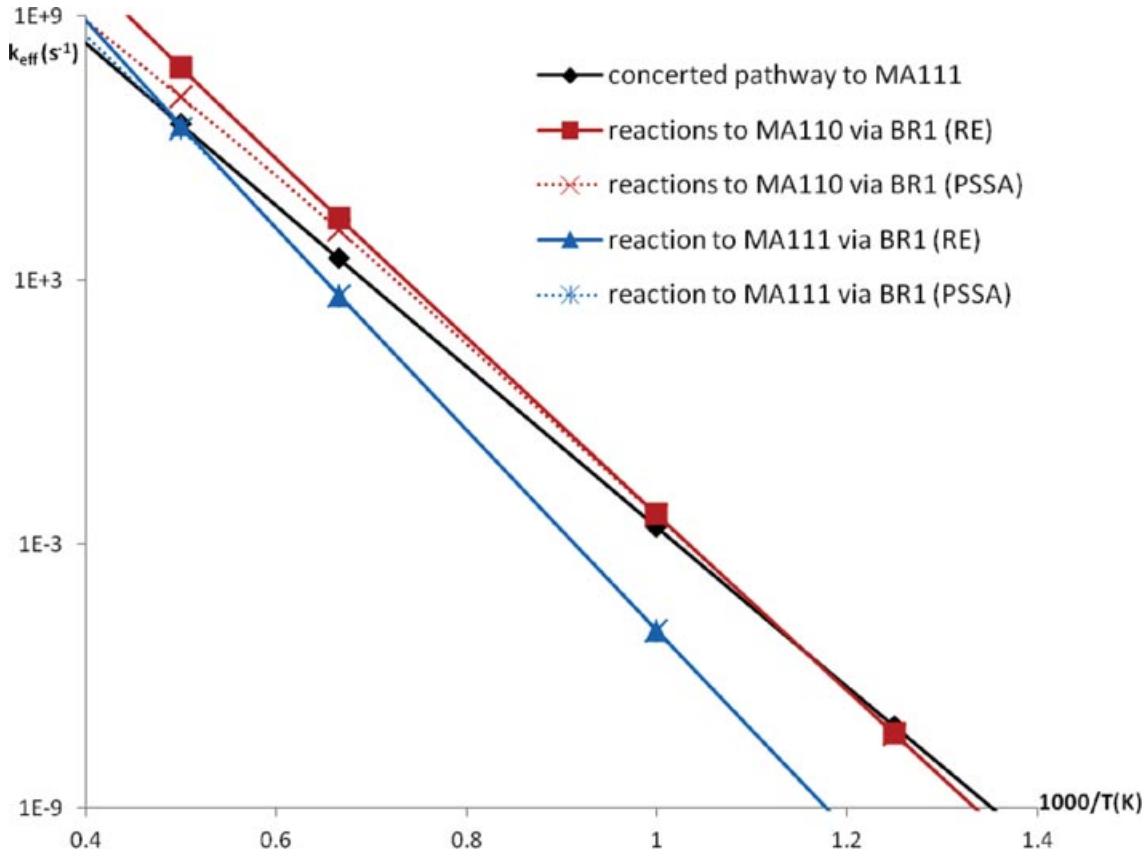

Figure 10 Effective rates for initial decomposition of JP-10 through various pathways (RE, rapid equilibrium assumption; PSSA, pseudo–steady-state approximation).

concerted reaction in the Arrhenius plots shown in Fig. 10 suggests that the activation energy for the concerted pathway is lower than the effective activation energy for the intramolecular disproportionation process (taking recombination and disproportionation of the biradical into consideration).

It should be noted that this comparison is particularly sensitive to both the Herbinet et al. kinetic parameters for the BR1 intramolecular disproportionation reactions (which, as the results of the section Intramolecular Disproportionation suggest, may be inaccurate) and the thermochemistry of JP-10 and BR1. For example, if the group additivity estimates for BR1 thermochemistry from Herbinet et al. are used in place of the BR1 quantum chemistry values from Herbinet et al., the concerted pathway appears to be noticeably less competitive, apparently largely due to the significant entropy discrepancy between the two estimates. This suggests that accurately capturing biradical thermochemistry will be an important consideration in future efforts to refine JP-10 decomposition models.

It should also be noted that it has recently been proposed that ring opening via carbenes may be competitive with biradical routes [51], but the issue is far from settled. These carbene pathways have not been considered here.

CONCLUSIONS

Multireference (CASSCF and MCQDPT) and CR-CC(2,3) calculations have been applied to study the initial stages of JP-10 decomposition. Results of these studies demonstrate interesting method-dependent phenomena for the potential energy surfaces of disproportionation reactions and provide evidence that the barriers to these reactions may be much lower than previously thought in the case of intramolecular disproportionation in a key JP-10 decomposition pathway. The new calculations suggest that some disproportionation steps may be barrierless. Results of the MCQDPT and CR-CC(2,3) calculations that provide a balanced and accurate description of dynamical and

nondynamical many-electron correlation effects for chemical reaction pathways involving biradicals and that agree with one another suggest that the CASSCF approach that neglects dynamical correlations produces unphysical SP structures and unreliable reaction path energetics for intramolecular disproportionation processes. Modeling results suggest that the effect of reducing activation energies for the intramolecular disproportionation pathways would be to extend the time to ignition for conditions with the longest ignition delay. Our quantum chemical calculations have also identified previously unexplored pathways for JP-10 decomposition involving concerted ring-opening pathways that bypass biradical formation. Preliminary analysis suggests that these additional pathways are likely not quite competitive with the biradical pathways that are characterized (according to high-level MCQDPT and CR-CC(2,3) calculations) by low-energy barriers or lack of activation barriers, though they are not necessarily insignificant. Overall, our findings demonstrate that the chemistry of ring opening and associated pathways is not yet completely understood and further study is needed, and that a serious effort has to be made to incorporate the results of higher level ab initio quantum chemistry calculations accurately accounting for dynamical and nondynamical correlation effects to obtain reliable predictions.

The authors gratefully acknowledge program support by Mr. Richard Burnes. This work has also been supported by the dissertation completion fellowship awarded by Michigan State University to Jesse J. Lutz. Additionally, the authors gratefully acknowledge the procurement of high-performance computing resources by the Engineer Research and Development Center, Maui High-Performance Computing Center, and Air Force Research Laboratory DoD Supercomputing Resource Centers. Finally, helpful communications with Larry Harding regarding the Kiefer et al. paper are acknowledged.

SUPPORTING INFORMATION

Saddle-point geometries discussed in the text, as well as the reactant and product geometries that each saddle point connects, are included as electronic Supporting Information. Zero-point energies and imaginary frequencies are included in a spreadsheet. JP-10 combustion mechanism version 0.19 is also included as electronic Supporting Information in CHEMKIN format. All this Supporting Information is available in the online issue at wileyonlinelibrary.com.

BIBLIOGRAPHY

1. Mikolaitis, D. W.; Segal, C.; Chandy, A. J Propul Power 2003, 19, 601–606.
2. Bruno, T. J.; Huber, M. L.; Laesecke, A.; Lemmon, E. W.; Perkins, R. A. NISTIR 6640, 2006.
3. Colket, M. B.; Spadaccini, L. J. J Propul Power 2001, 17, 315–323.
4. Cooper, M.; Shepherd, J. E. Thermal and Catalytic Cracking of JP-10 for Pulse Detonation Engine Applications; GALCIT Report FM 2002.002; California Institute of Technology: Pasadena, CA, 2002.
5. Davidson, D. F.; Horning, D. C.; Herbon, J. T.; Hanson, R. K. Proc Combust Inst 2000, 28, 1687–1692.
6. Green, R. J.; Anderson, S. L. In Proceedings of the 13th ONR Propulsion Meeting, Salt Lake City, UT, 2000.
7. He, K. Y.; Androulakis, I. P.; Ierapetritou, M. G. Energy Fuels 2010, 24, 309–317.
8. Herbinet, O.; Sirjean, B.; Bounaceur, R.; Fournet, R.; Battin-Leclerc, F.; Scacchi, G.; Marquaire, P. M. J Phys Chem A 2006, 110, 11298–11314.
9. Li, S. C.; Varatharajan, B.; Williams, F. A. AIAA J 2001, 39, 2351–2356.
10. Magoon, G. R.; Green, W. H.; Oluwole, O. O.; Wong, H.-W.; Albo, S. E.; Lewis, D. K. In 46th AIAA/ASME/SAE/ASEE Joint Propulsion Conference & Exhibit, Nashville, TN, 2010.
11. Van Devener, B.; Anderson, S. L. Energy Fuels 2006, 20, 1886–1894.
12. Allen, J. W.; Ashcraft, R. W.; Beran, G. J.; Goldsmith, C. F.; Harper, M. R.; Jalan, A.; Magoon, G. R.; Matheu, D. M.; Petway, S.; Sumathy, R.; Sharma, S.; Van Geem, K. M.; Song, J.; Wen, J.; West, R. H.; Wong, A.; Wong, H.-W.; Yelvington, P. E.; Yu, J.; Green, W. H. RMG (reaction mechanism generator), 2009.
13. Lutz, A. E.; Kee, R. J.; Miller, J. A. SENKIN: A FORTRAN program for predicting homogeneous gas phase chemical kinetics with sensitivity analysis, in Sandia National Lab report 87-8248, 1987.
14. Kee, R. J.; Rupley, F. M.; Miller, J. A.; Coltrin, M. E.; Grcar, J. F.; Meeks, E.; Moffat, H. K.; Lutz, A. E.; Dixon-Lewis, G.; Smooke, M. D.; Warnatz, J.; Evans, G. H.; Larson, R. S.; Mitchell, R. E.; Petzold, L. R.; Reynolds, W. C.; Caracotsios, M.; Stewart, W. E.; Glarborg, P.; Wang, C.; McLellan, C. L.; Adigun, O.; Houf, W. G.; Chou, C. P.; Miller, S. F.; Ho, P.; Young, P. D.; Young, D. J.; Hodgson, D. W.; Petrova, M. V.; Puduppakkam, K. V. CHEMKIN Release 4.1.1, Reaction Design: San Diego, CA, 2007.
15. Roos, B. O. Adv Chem Phys 1987, 69, 399–445, and references therein.
16. Roos, B. O.; Taylor, P. R. Chem Phys 1980, 48, 157–173.
17. Schmidt, M. W.; Gordon, M. S. Annu Rev Phys Chem 1998, 49, 233–266.
18. Nakano, H. Chem Phys Lett 1993, 207, 372–378.
19. Nakano, H. J Chem Phys 1993, 99, 7983–7992.
20. Piecuch, P.; Włoch, M. J Chem Phys 2005, 123, 224105.

21. Piecuch, P.; Włoch, M.; Gour, J. R.; Kinal, A. Chem Phys Lett 2006, 418, 467–474.
22. Włoch, M.; Gour, J. R.; Piecuch, P. J Phys Chem A 2007, 111, 11359–11382.
23. Włoch, M.; Lodriguito, M. D.; Piecuch, P.; Gour, J. R. Mol Phys 2006, 104, 2149–2172.
24. Purvis, G. D.; Bartlett, R. J. J Chem Phys 1982, 76, 1910–1918.
25. Cramer, C. J.; Kinal, A.; Włoch, M.; Piecuch, P.; Gagliardi, L. J Phys Chem A 2006, 110, 11557–11568.
26. Cramer, C. J.; Włoch, M.; Piecuch, P.; Puzzarini, C.; Gagliardi, L. J Phys Chem A 2006, 110, 1991–2004.
27. Ge, Y. B.; Gordon, M. S.; Piecuch, P. J Chem Phys 2007, 127, 174106.
28. Ge, Y. B.; Gordon, M. S.; Piecuch, P.; Włoch, M.; Gour, J. R. J Phys Chem A 2008, 112, 11873–11884.
29. Kinal, A.; Piecuch, P. J Phys Chem A 2007, 111, 734–742.
30. Song, Y. Z.; Kinal, A.; Caridade, P. J. S. B.; Varandas, A. J. C.; Piecuch, P. J Mol Struct: THEOCHEM 2008, 859, 22–29.
31. Piecuch, P.; Włoch, M.; Varandas, A. J. C. Theor Chem Acc 2008, 120, 59–78.
32. Becke, A. D. J Chem Phys 1993, 98, 5648–5652.
33. Lee, C. T.; Yang, W. T.; Parr, R. G. Phys Rev B 1988, 37, 785–789.
34. Krishnan, R.; Binkley, J. S.; Seeger, R.; Pople, J. A. J Chem Phys 1980, 72, 650–654.
35. Montgomery, J. A.; Frisch, M. J.; Ochterski, J. W.; Petersson, G. A. J Chem Phys 1999, 110, 2822–2827.
36. Frisch, M. J.; Trucks, G. W.; Schlegel, H. B.; Scuseria, G. E.; Robb, M. A.; Cheeseman, J. R.; Scalmani, G.; Barone, V.; Mennucci, B.; Petersson, G. A.; Nakatsuji, H.; Caricato, M.; Li, X.; Hratchian, H. P.; Izmaylov, A. F.; Bloino, J.; Zheng, G.; Sonnenberg, J. L.; Hada, M.; Ehara, M.; Toyota, K.; Fukuda, R.; Hasegawa, J.; Ishida, M.; Nakajima, T.; Honda, Y.; Kitao, O.; Nakai, H.; Vreven, T.; Montgomery, J. J. A.; Peralta, J. E.; Ogliaro, F.; Bearpark, M.; Heyd, J. J.; Brothers, E.; Kudin, K. N.; Staroverov, V. N.; Kobayashi, R.; Normand, J.; Raghavachari, K.; Rendell, A.; Burant, J. C.; Iyengar, S. S.; Tomasi, J.; Cossi, M.; Rega, N.; Millam, N. J.; Klene, M.; Knox, J. E.; Cross, J. B.; Bakken, V.; Adamo, C.; Jaramillo, J.; Gomperts, R.; Stratmann, R. E.; Yazyev, O.; Austin, A. J.; Cammi, R.; Pomelli, C.; Ochterski, J. W.; Martin, R. L.; Morokuma, K.; Zakrzewski, V. G.; Voth, G. A.; Salvador, P.; Dannenberg, J. J.; Dapprich, S.; Daniels, A. D.; Farkas, Ö.; Foresman, J. B.; Ortiz, J. V.; Cioslowski, J.; Fox, D. J. Gaussian 09, Revision A.02; Gaussian, Inc.: Wallingford, CT, 2009.
37. Gordon, M. S.; Schmidt, M. W. In Theory and Applications of Computational Chemistry, the First Forty Years; Dykstra, C. E.; Frenking, G.; Kim, K. S.; Scuseria, G. E., Eds.; Elsevier: Amsterdam, the Netherlands, 2005; pp. 1167–1189.
38. Schmidt, M. W.; Baldridge, K. K.; Boatz, J. A.; Elbert, S. T.; Gordon, M. S.; Jensen, J. H.; Koseki, S.; Matsunaga, N.; Nguyen, K. A.; Su, S. J.; Windus, T. L.; Dupuis, M.; Montgomery, J. A. J Comput Chem 1993, 14, 1347–1363.
39. Piecuch, P.; Kucharski, S. A.; Kowalski, K.; Musial, M. Comput Phys Commun 2002, 149, 71–96.
40. Bode, B. M.; Gordon, M. S. J Mol Graphics Modell 1998, 16, 133–138.
41. Malick, D. K.; Petersson, G. A.; Montgomery, J. A. J Chem Phys 1998, 108, 5704–5713.
42. Zheng, J.; Gour, J. R.; Lutz, J. J.; Włoch, M.; Piecuch, P.; Truhlar, D. G. J Chem Phys 2008, 128, 044108.
43. Mousavipour, S. H.; Homayoon, Z. J Phys Chem A 2003, 107, 8566–8574.
44. Zhu, R. S.; Xu, Z. F.; Lin, M. C. J Chem Phys 2004, 120, 6566–6573.
45. Sirjean, B.; Glaude, P. A.; Ruiz-Lopez, M. F.; Fournet, R. J Phys Chem A 2006, 110, 12693–12704.
46. Kiefer, J. H.; Gupte, K. S.; Harding, L. B.; Klippenstein, S. J. J Phys Chem A 2009, 113, 13570–13583.
47. Izgorodina, E. I.; Coote, M. L.; Radom, L. J Phys Chem A 2005, 109, 7558–7566.
48. Ventura, E.; Dallos, M.; Lischka, H. J Chem Phys 2003, 118, 10963–10972.
49. Szalay, P. G.; Bartlett, R. J. Chem Phys Lett 1993, 214, 481–488.
50. Sharma, S.; Harper, M. R.; Green, W. H. CANTHERM v1.0, 2010.
51. Dames, E.; Krylov, A.; Wang, H. In 7th U.S. National Technical Meeting of the Combustion Institute, Atlanta, GA, 2011.